5.3 Background sources and asymmetries

In the early SLD runs, when a purely calorimetric event selection procedure was used, beam/machine related noise represented a major contribution to the A_{LR} background. With the introduction of the tracking-assisted algorithm described here, and improvements in the beam transport scheme, this background was essentially eliminated. The residual background in the Z^0 sample can now be attributed to two sources: wide angle Bhabhas and two-photon events. The latter can only make it into the sample when they coincide with machine related backgrounds.

In 1997/98, we were able to resolve outstanding problems with the SLD production Monte Carlo and achieve good agreement with the data for all parameters that might affect the A_{LR} event selection [49]. This made it possible to use Monte Carlo directly to estimate the residual background in our Z^0 sample. Old data-driven techniques were still used as a cross check. The background fraction caused by the two-photon events was calculated to be 0.016 % for the 1996 run, and 0.029 % for the 1997/98 run. The background fraction due to the WAB events was 0.013 % for both runs. We conservatively assign a systematic error equal to the background fraction itself to these results.

Unlike other backgrounds, the background due to WABs has a left-right asymmetry of its own, since it consists of s-channel Z exchange events (which have asymmetry identical to that of hadronic events and are not actually a background) as well as of t-channel photon exchange, $\gamma - Z$ interference, and other events. Hence, the correction to

the measured asymmetry in Z^0 production due to background is calculated as $f_b(A_m - A_b)$, where A_m is the measured asymmetry, A_b is the background asymmetry, and f_b is the total background fraction. Because WABs are the only part of the background that has a sizeable left-right asymmetry, A_b is approximately equal to wA_w, where w is the fraction of the background due to WABs, and A_w is the WAB asymmetry determined from Monte Carlo.

5.4 Summary

Table 5.1 summarizes the results of the event selection for all SLD runs, and presents the measured values of the left-right asymmetry in Z^0 production. It should be noted that systematic errors due to the background are much smaller than the polarimetry and energy scale related uncertainties.

5.5 Cross checks

As a cross check, we verified that the measured asymmetry A_m was not affected significantly when we applied considerably more restrictive selection criteria to our data sample. We also checked that A_m was uniform when calculated separately for different values of parameters used in the event selection. Figures 5.6 and 5.7 show the measured asymmetry for as a function of the energy imbalance and the number of tracks, respectively, for the 1997/98 run data sample.

We also verified that A_m was uniform when binned by the azimuth and polar angle

Table 5.1: Z^0 event selection results and background estimates for all SLD runs. Note: the background asymmetry for the 1992 run was not estimated and assumed to be zero when calculating the size of the correction to the measured asymmetry. The assumption is reasonable given the dominance of the machine/beam related background during that run. The overall systematic error was inflated to include the uncertainty in the background asymmetry.

	1992	1993	1994/95	1996	1997/98
Number of Z^0 bosons produced with left-handed electron beam, N_L	5,226	27,225	52,179	29,016	183,335
Number of Z^0 bosons produced with right-handed electron beam, N_R	4,998	22,167	41,465	22,857	148,259
Measured asymmetry, A_m	0.0223 $\pm$0.0099	0.1024 $\pm$0.0045	0.1144 $\pm$0.0032	0.1187 $\pm$0.0044	0.1058 $\pm$0.0017
Selection efficiency before polarization matching, per cent	90 $\pm$2	93 $\pm$1	89.3 $\pm$0.8	91.9 $\pm$0.9	91.0 $\pm$0.9
Selection efficiency after polarization matching, per cent	88 $\pm$2	91 $\pm$1	86.0 $\pm$0.8	91.4 $\pm$1.0	89.8 $\pm$0.9
Background fraction f_b, per cent	1.4 $\pm$1.4	0.25 $\pm$0.10	0.11 $\pm$0.08	0.029 $\pm$0.021	0.042 $\pm$0.032
Background asymmetry A_b		0.031 $\pm$0.010	0.055 $\pm$0.021	0.033 $\pm$0.026	0.023 $\pm$0.022

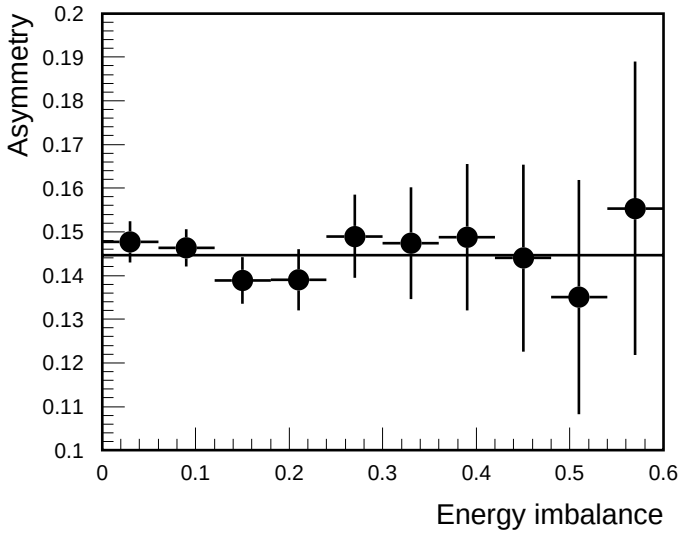

Figure 5.6: Measured asymmetry in Z^0 production binned by the energy imbalance. 1997/98 data sample. Confidence level for a horizontal straight line fit is 63 %.

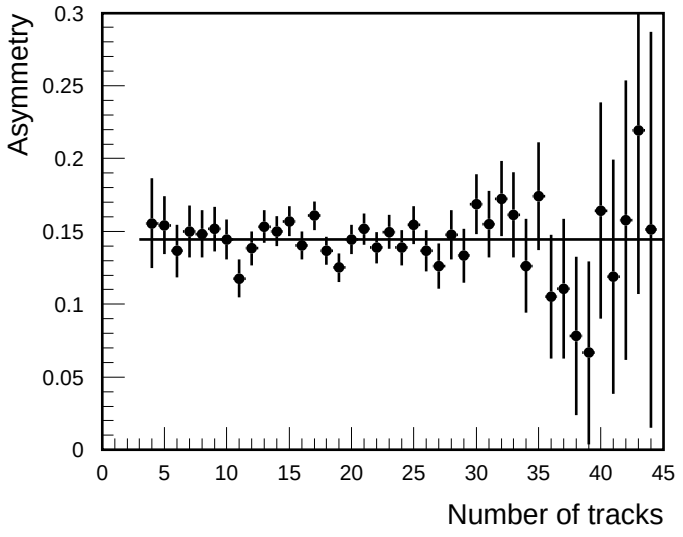

Figure 5.7: Measured asymmetry in Z^0 production binned by the track multiplicity. 1997/98 data sample.

of the thrust axis. The distribution for the polar angle is shown in figures 5.8.

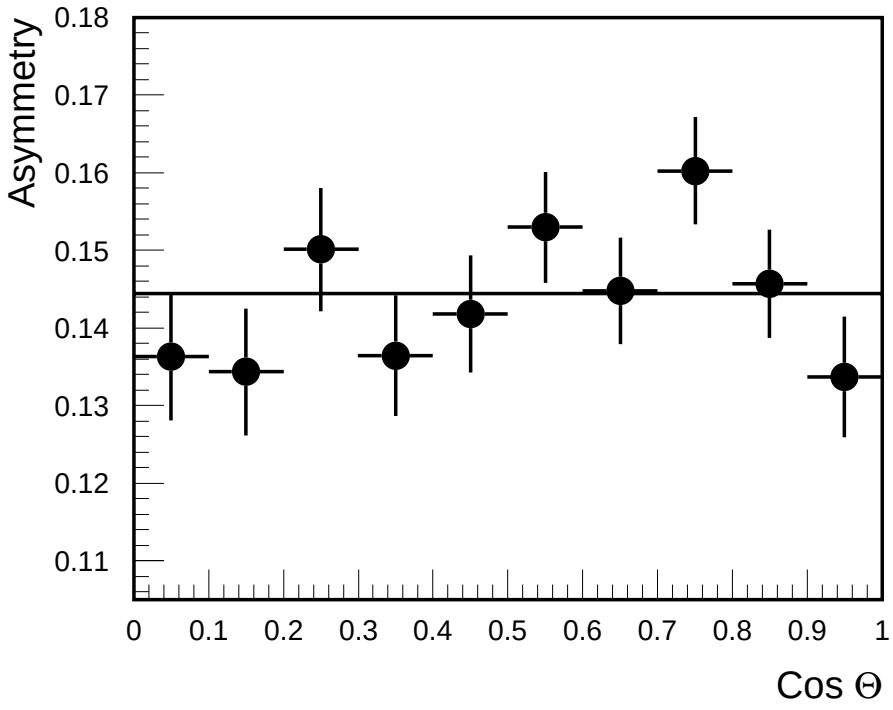

Figure 5.8: Measured asymmetry in Z^0 production binned by the polar angle of the thrust axis. 1997/98 data sample. Confidence level for a horizontal straight line fit is 17 %.

Chapter 6

Extracting A_{LR}^0 from the measured asymmetry in Z^0 production

6.1 Instrumental asymmetries and additional corrections

The measured asymmetry A_m is related to A_{LR} by the following expression, which takes into account a number of small corrections in their lowest order approximations:

$$A_{LR} = \frac{A_m}{\mathcal{P}_e} + \frac{1}{\mathcal{P}_e}\left[f_b(A_m - A_b) - A_{\mathcal{L}} + A_m^2 A_{\mathcal{P}} - E_{cm}\frac{\sigma'(E_{cm})}{\sigma(E_{cm})}A_E - A_\varepsilon + \mathcal{P}_e\mathcal{P}_p\right] \quad (6.1)$$

where $\mathcal{P}_e$ is the luminosity-weighted polarization; f_b and A_b are the background fraction and asymmetry; $A_{\mathcal{L}}$, $A_{\mathcal{P}}$, A_E, and A_ε are the left-right asymmetries of the integrated

luminosity, the electron beam polarization, the center-of-mass energy, and the detection efficiency, respectively; $\sigma(E_{cm})$ is the unpolarized Z^0 cross section at the average center-of-mass energy E_{cm}, and $\sigma'(E_{cm})$ is its derivative with respect to E at the same energy; $\mathcal{P}_p$ is the average longitudinal positron polarization.

The term describing the correction due to the residual background in the Z^0 sample was discussed in the previous chapter.

The polarization asymmetry $A_{\mathcal{P}}$ is measured directly by the polarimeter, by calculating the observed asymmetry in Compton scattering separately for machine pulses with left and right handed beams (this is possible because the laser helicity sign is also changed randomly from pulse to pulse).

From the detection point of view, the only difference between left and right handed Z^0s is that the distributions of outgoing fermions are reversed in the polar angle with respect to the electron beam direction. Therefore, the detection asymmetry A_ε should vanish if the detector acceptance and efficiency are either symmetric in the polar angle, or equal for fermions and anti-fermions at any given polar angle. Both conditions are true for the SLD detector, which implies negligible correction due to the A_ε.

The luminosity and energy asymmetries are both studied [50, 51] using the so called "120 Hz" data stream. Since 1993, in addition to physics-triggered events, the SLD has been writing to tape a small set of important detector and accelerator parameters for each of the machine pulses. These parameters include, among others, the readings from the BeamStrahlung Monitor (BSM), beam current toroids, WISRD energy

spectrometers, and the North Final Focus Radiative Bhabha Detector (NFF Lum).

The NFF Lum directly measures the relative luminosity and therefore $A_{\mathcal{L}}$, which was found to be consistent with being caused mainly by the asymmetry in the electron beam current, which is monitored by the toroids. The positron beam current asymmetry was consistent with zero, as expected, since the positron bunch was produced one machine cycle earlier than the electron bunch it collided with. Given that the electron polarization changes sign randomly from pulse to pulse, the positron beam current should be completely uncorrelated to the electron beam polarization sign.

The A_E is directly measured by the WISRDs. The electron beam energy was found to be anti-correlated with its current, in quantitative agreement with the assumption that the effect is caused by the so-called "beam loading" of the accelerating structure: the bigger the current of the bunch, the smaller the acceleration it receives.

Because both the luminosity and the center-of-mass energy asymmetries are caused by the electron beam current asymmetry, it was possible to substantially reduce the integrated size of both $A_{\mathcal{L}}$ and A_E by reversing the LINAC-TO-RING spin rotator (LTR), located at the entry to the SLC damping ring (see section 3.1 for details), several times during each SLD run. Since the beam current asymmetry is produced by the SLC polarized electron source, reversing the LTR (which results in changing the polarization sign at the SLD IP) causes the $A_{\mathcal{L}}$ and A_E to change sign also. The coefficient before A_E in equation 6.1 is a sensitive function of energy, and is calculated using the measured luminosity-weighted center-of-mass energy (see table 3.3).

Prior to 1998, we always assumed that the correction due to the positron beam polarization was negligible. Note that in order to cause any effect on the A_{LR}, the polarization should have constant helicity. Any residual positrons polarization resulting from the helicity of the electron bunch used in their production would be uncorrelated to the electron beam polarization because, as was mentioned above, electrons and positrons are produced in different machine cycles, and the electron beam polarization changes sign randomly. The dominant potential source of positron polarization of constant helicity is the Sokolov-Ternov effect [52] in the positron damping ring, and the resulting polarization was calculated to be less than $1.6 \cdot 10^{-5}$, which implies negligible correction to the A_{LR}.

To verify this assumption experimentally, the positron polarization was directly measured immediately after the SLD 1997/98 run by delivering the positron beam to the fixed target Møller polarimeter in the End Station A. The measured polarization was found to be -0.0002 ± 0.0007 [53], consistent with zero as expected.

Table 6.1 provides a summary of corrections to the measured left-right asymmetry in Z_0 production that enter equation 6.1. It should be noted that the total correction and its associated systematic error are small compared to the polarization measurement uncertainty.

Table 6.1: A_{LR} calculation: summary of corrections to the measured asymmetry in Z^0 production. In the 1992 run analysis, no corrections were applied to the central value of the A_{LR}. Instead, they were included in the estimate of the systematic uncertainty. The A_E correction for that year was estimated to be negligible compared to other terms.

	1992	1993	1994/95	1996	1997/98
Luminosity asymmetry, $A_{\mathcal{L}}$, (10^{-4})	1.8 ± 4.2	0.38 ± 0.50	-1.9 ± 0.3	$+0.03 \pm 0.50$	-1.3 ± 0.7
Polarization asymmetry, $A_{\mathcal{P}}$, (10^{-4})	-29	-33 ± 1	$+24 \pm 10$	$+29 \pm 43$	$+28 \pm 69$
Center-of-mass energy asymmetry, A_E, (10^{-4})		0.0044 ± 0.0001	0.0092 ± 0.0002	-0.0001 ± 0.0035	$+0.0028 \pm 0.0014$
$E_{cm}\frac{\sigma'(E_{cm})}{\sigma(E_{cm})}$		-1.9	0.0 ± 2.5	2.0 ± 3.0	4.3 ± 2.9
Detection efficiency asymmetry, A_ε	0	0	0	0	0
Positron beam polarization $\mathcal{P}_p$, (10^{-4})	< 0.16	< 0.16	< 0.16	< 0.16	-2 ± 7
Total correction, $\Delta A_{LR}/A_{LR}$, (%)		$+0.10 \pm 0.08$	$+0.2 \pm 0.06$	$+0.02 \pm 0.05$	$+0.16 \pm 0.07$

6.2 A_{LR}^0 calculation

We now have all ingredients required for calculating the A_{LR} using equation 6.1. The measured asymmetry A_m can be found in table 5.1. The luminosity-weighted electron beam polarization $\mathcal{P}_e$ is given in table 3.6. The corrections to the measured asymmetry are listed in table 6.1.

To convert the measured A_{LR} to its Z-pole value, we use the measured value of the luminosity-weighted average center-of-mass energy given in table 3.3, and the ZFITTER program [16], which takes into account the initial state radiation, the photon exchange, and the electroweak interference, as described in chapter 2. The effective weak mixing angle can be determined by reversing the equation

$$A_{LR}^0 = \frac{2(1-4sin^2\theta_W^{eff})}{1+(1-4sin^2\theta_W^{eff})^2} \tag{6.2}$$

The results are presented in table 6.2. The grand averages for the complete SLD data sample are:

$$A_{LR}^0 = 0.15138 \pm 0.00216$$

$$sin^2\theta_W^{eff} = 0.23097 \pm 0.00027$$

Table 6.2: A_{LR} and $sin^2\theta_W^{eff}$ measurements: summary of results for all SLD runs. Statistical errors are listed first.

	A_{LR}	A_{LR}^0	$sin^2\theta_W^{eff}$
1992	0.100 $\pm 0.044 \pm 0.004$	0.097 $\pm 0.044 \pm 0.004$	0.2378 $\pm 0.0056 \pm 0.0005$
1993	0.1628 $\pm 0.0071 \pm 0.0028$	0.1656 $\pm 0.0071 \pm 0.0028$	0.2292 $\pm 0.0009 \pm 0.0004$
1994/95	0.1485 $\pm 0.0042 \pm 0.0010$	0.1512 $\pm 0.0042 \pm 0.0011$	0.23100 $\pm 0.00054 \pm 0.00014$
1996	0.1559 $\pm 0.00572 \pm 0.00084$	0.15929 $\pm 0.00573 \pm 0.00101$	0.22996 $\pm 0.00073 \pm 0.00013$
1997/98	0.1454 $\pm 0.00237 \pm 0.00077$	0.14906 $\pm 0.00237 \pm 0.00096$	0.23126 $\pm 0.00030 \pm 0.00012$
All combined		0.15138 ± 0.00216	0.23097 ± 0.00027

Chapter 7

Results and conclusions

7.1 Comparison with other measurements

The A_{LR}^0 measurements performed during the 5 different SLD runs (table 6.2) are consistent with each other and yield the average value of $A_{LR}^0 = A_e = 0.15138 \pm 0.00216$.

In addition to the A_{LR}^0, the SLD experiment determines polarized left-right forward-backward asymmetries $\tilde{A}_{FB}^f$ (see section 2.5) for leptonic final states, thus providing direct measurements of A_e, A_μ, and A_τ [54]. Since the e^+e^- final states are treated as a background in the A_{LR}^0 analysis (chapter 5), the A_e values extracted from the $\tilde{A}_{FB}^e$ and the A_{LR}^0 are statistically independent, and can be combined, taking into account correlation between their systematic errors due to uncertainties in the electron beam polarization and the center-of-mass energy measurements, which affect both analyses. The average is dominated by the significantly more precise A_{LR}^0 measurement. The combined results based on the complete SLD data sample are

$$A_e = 0.1516 \pm 0.0021$$

$$A_\mu = 0.142 \pm 0.015$$

$$A_\tau = 0.136 \pm 0.015$$

Assuming lepton universality and combining the above results, we obtain the average of $A_l = 0.15130 \pm 0.00207$, which is equivalent to the effective weak mixing angle of $\sin^2\theta_W^{eff} = 0.23098 \pm 0.00026$. Once again, small common systematic effects have been taken into account.

The four LEP experiments (ALEPH, DELPHI, L3, and OPAL) determine the effective weak mixing angle through the measurements of unpolarized forward-backward asymmetries described in section 2.5. Figure 7.1 presents the comparison of the world average $\sin^2\theta_W^{eff}$ values extracted from different observables. The global average is $\sin^2\theta_W^{eff} = 0.23150 \pm 0.00017$, with the results of the different groups of measurements being marginally consistent: $\chi^2 = 13.1/7$ d.o.f. The two most precise measurements, A_{LR}^0 and $A_{FB}^{(0,b)}$, disagree by about 3 σ. It is interesting to note that the agreement is excellent within each of the two groups of measurements, corresponding to leptonic and hadronic final states.

A convenient way to compare the results with the Electroweak Standard Model predictions is to use the S,T,U parameters of Peskin and Takeuchi [55], which parameterize oblique (vacuum polarization) corrections to the gauge boson propagators. New physics may manifest itself through small deviations of these parameters from their Standard Model values, since the corrections would be sensitive to the existence of new heavy

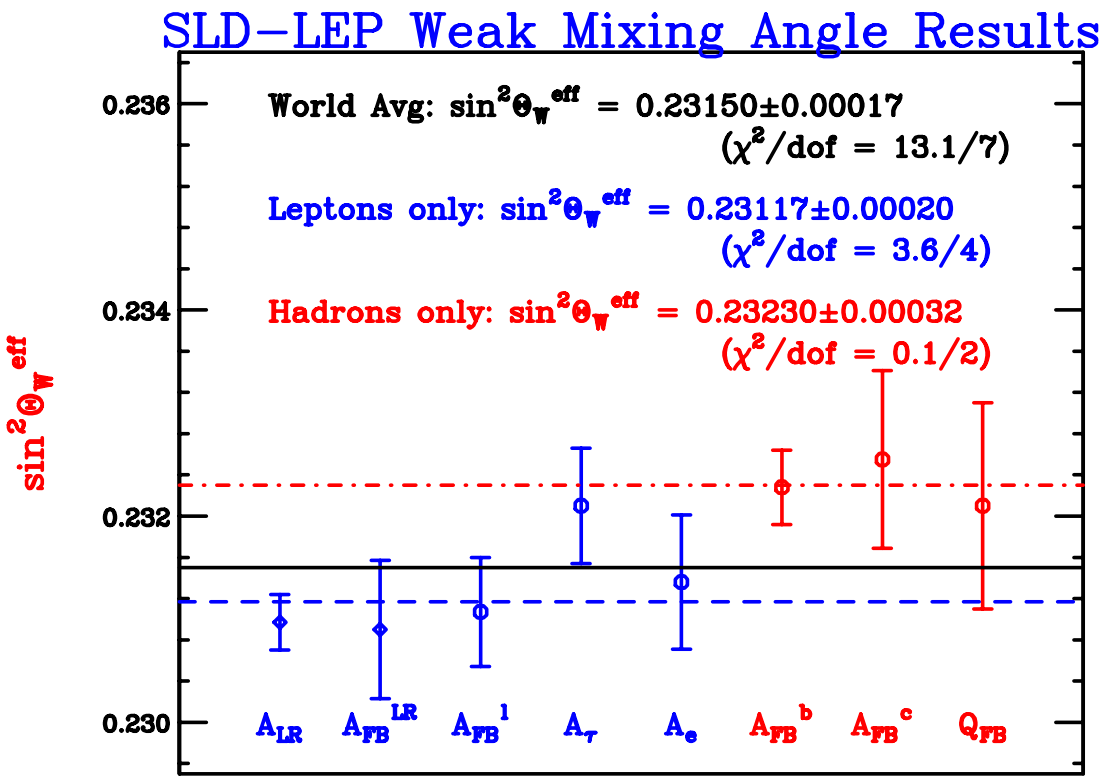

Figure 7.1: Comparisons of several determinations of $\sin^2\theta_W^{eff}$ from electroweak asymmetries. Based on the LEP and the SLD results.

particles. Each observable can be expanded to the first order in S,T,U (the expansion coefficients are calculated in [55], and are independent of M_H and m_t).

In figure 7.2, the confidence bands corresponding to the expansions of three precisely measured observables ($\sin^2\theta_W^{eff}$, M_W, and Γ_Z) are shown in the S-T plane (U=0), since the neutral current observables are independent of U. The Standard Model prediction is shown as a band corresponding to a range of the Higgs boson masses, with it's width reflecting the uncertainty in the top quark mass. The data is in good agreement with the model, with lighter Higgs being favored.

7.2 Conclusion

The A_{LR}^0 measurement described in this thesis is the world's most precise single experiment determination of the effective weak mixing angle, $\sin^2\theta_W^{eff}$. Since there are still unanswered questions in the electroweak theory, and the results of the $\sin^2\theta_W^{eff}$ measurements by various experiments are only marginally consistent, further experimental study of this issue would have a substantial discovery potential. Several proposals to measure the A_{LR}^0 at either TESLA [56] or NLC [57] are currently being discussed. These machines can in principle provide much higher Z^0 statistics than the SLD detector collected. However, in order to achieve substantial improvement in the $\sin^2\theta_W^{eff}$ determination accuracy, the experiments will have to address a number of experimental issues similar to those we had to deal with at the SLD, but at a higher level of precision. We therefore hope the experience gained by the SLD collaboration will be valuable for

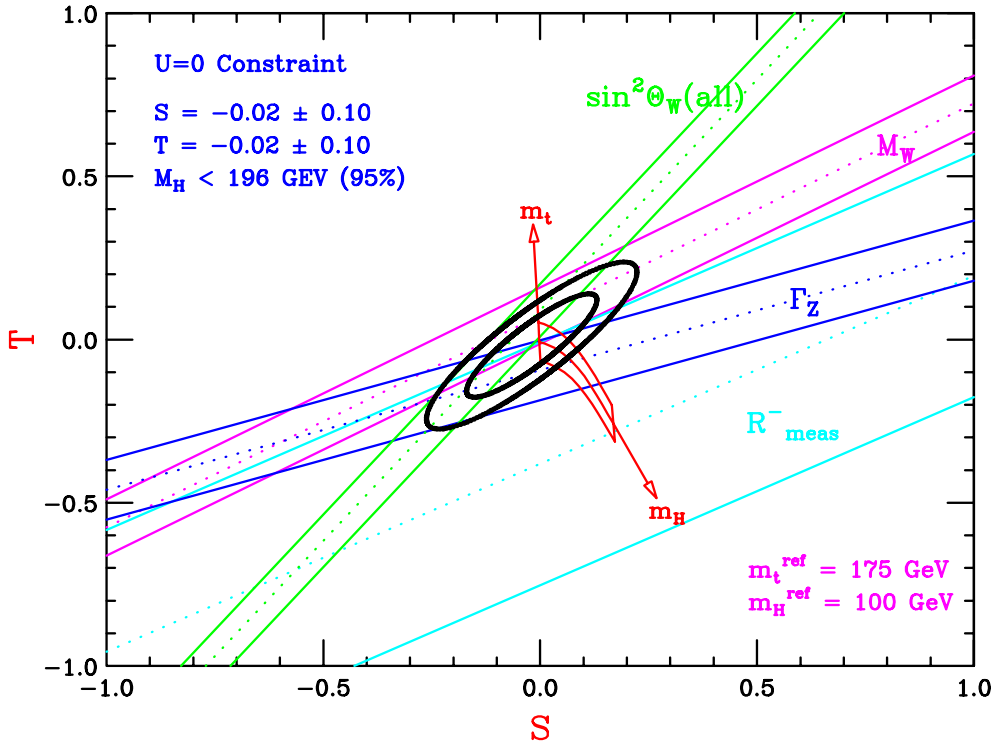

Figure 7.2: Electroweak measurements and the Standard Model predictions - ST parameters plot.

planning and designing these experiments.

Since the beam polarization measurement is likely to be one of the most critical issues, the calorimeter-based polarimeter technique that has been developed is particularly important.

The Quartz Fiber Calorimeter has become the first successful implementation of this technique, and played an important role in achieving the high accuracy of the A_{LR}^0 measurement at the SLD. Using the quartz fiber technology allowed to design a detector capable of operating in the complicated environment of the SLC Final Focus, which required an extreme radiation hardness, insensitivity to soft synchrotron radiation, small size, high linearity, and position resolution. The target sub-1 % accuracy of the polarization measurement was achieved without interfering with the operation of other detectors located in the polarimeter area, and with minimal interruption of the physics data taking by the SLD detector. We anticipate that future polarimeters based on this technique will be able to provide significantly better accuracy of the longitudinal polarization measurement, and to measure the transverse polarization of the electron beam. To achieve this, it is critical to design the beam layout with the polarimeter in mind, and allocate sufficient time for the polarimeter study and tune-up.

Bibliography

Bibliography

[1] R. King. *A Precise Measurement of the Left-Right Asymmetry of Z Boson Production at the SLAC Linear Collider.* PhD thesis, Stanford University, 1994.

[2] A. Lath. *A Precise Measurement of the Left-Right Cross Section Asymmetry in Z Boson Production.* PhD thesis, Massachusetts Institute of Technology, 1994.

[3] R. Elia. Measurement of the left-right asymmetry in Z boson production by electron-positron collisions. SLAC-Report 429, Stanford Linear Accelerator Center, 1994.

[4] K. Abe et al. First measurement of the left-right cross section asymmetry in z boson production by e^+e- collisions. *Physical Review Letters*, 70:2515–2520, 1993.

[5] K. Abe et al. Precise measurement of the left-right cross section asymmetry in z boson production by e^+e- collisions. *Physical Review Letters*, 73:25–29, 1994.

[6] K. Abe et al. Improved measurement of the left-right z^0 cross section asymmetry. *Physical Review Letters*, 78:2075–2079, 1997.

[7] C. Prescott. Spin dependent Compton scattering for use in analyzing electron beam polarizations. SLAC-TN 73-1, Stanford Linear Accelerator Center, 1973.

[8] M. Fero et al. Proposal for a Compton XYZ polarimeter for SLC. SLAC Memorandum, Stanford Linear Accelerator Center, 1993.

[9] P. H. Bucksbaum E. D. Commins. *Weak Interactions of Leptons and Quarks.* Cambridge University Press, 1983.

[10] D. V. Schroeder M. E. Peskin. *Quantum Field Theory.* Addison-Wesley Publishing Company, 1995.

[11] S. L. Glashow. *Nucl. Phys.*, 22:579, 1961.

[12] S. Weinberg. *Phys. Rev. Letters*, 19:1264, 1967.

[13] A. Salam. In *8th NOBEL Symposium*, page 367, 1968.

[14] V. S. Fadin E. A. Kuraev. *Sov. J. Nucl. Phys.*, 41:466, 1985.

[15] M. Swartz. Radiative corrections to electroweak measurements. SLD-Physics-Note 48, Stanford Linear Accelerator Center, 1996.

[16] D. Bardin et al. CERN-TH 6443/92, CERN, 1992.

[17] M. Woods. The polarized electron beam for the SLAC Linear Collider. In *Proceedings of the 12th International Symposium on High Energy Spin Physics. Amsterdam, The Netherlands.*, 1996.

[18] R. Alley et al. The Stanford Linear Accelerator polarized electron source. *Nucl. Instrum. Meth.*, A365:1–27, 1995.

[19] S.Watson M. Levi, J. Nash. Precision measurements for the SLC spectrometer magnets. SLAC-PUB 4654, Stanford Linear Accelerator Center, 1986.

[20] G. Blaylock. The WISRD beam energy measurement. SLD-Physics-Note 22, Stanford Linear Accelerator Center, 1993.

[21] LEP Electroweak Working Group. A combination of preliminary electroweak measurements and constraints on the standard model. CERN-EP 99-15, CERN, 1999.

[22] P. Rowson et al. Calibration of the WISRD spectrometer with a Z peak scan. SLD-Note 264, Stanford Linear Accelerator Center, 1999.

[23] R. Kofler G. Blaylock, S. Hertzbach. WISRD instrumental effects. Work in progress.

[24] R. Ben-David et al. Event selection and background estimation for the 1993 A_{LR} result. SLD-Note 243, Stanford Linear Accelerator Center, 1994.

[25] R. Kleiss F. Berends, W. Hollik. *Nucl. Phys.*, B304:712, 1988.

[26] Martin Breidenbach. Overview of the SLD. *IEEE Trans. Nucl. Sci.*, 33:46–50, 1986.

[27] M. D. Hildreth et al. Performance of the SLD central drift chamber. *IEEE Trans. Nucl. Sci.*, 42:451–458, 1995.

[28] K. Abe et al. Design and performance of the SLD vertex detector, a 307 Mpixel tracking system. *Nucl. Instrum. Meth.*, A400:287–343, 1997.

[29] D. Axen et al. The lead liquid argon sampling calorimeter of the SLD detector. *Nucl. Instrum. Meth.*, A328:472–494, 1993.

[30] A. C. Benvenuti et al. The iron calorimeter and muon identifier for SLD. *Nucl. Instr. Meth.*, A276:94, 1989.

[31] K. Abe et al. Performance of the CRID at SLD. *Nucl. Instrum. Meth.*, A343:74–86, 1994.

[32] P. L. Reinertsen. Higher order corrections to polarized compton scattering cross section and asymmetry. SLD-Physics-Note 46, Stanford Linear Accelerator Center, 1995.

[33] M. Woods A. Lath. Compton laser analysis: Determination of polarization and systematic errors. SLD-Note 236, Stanford Linear Accelerator Center, 1994.

[34] M. Woods et al. Compton laser analysis for the 94/95 sld run. SLD-Note 246, Stanford Linear Accelerator Center, 1996.

[35] J. P. Fernandez. Determination of the Compton polarimeter laser polarization for the 1996 SLD run. SLD-Note 257, Stanford Linear Accelerator Center, 1997.

[36] J. P. Fernandez. Determination of the Compton polarimeter laser polarization for the 1997/98 sld run. SLD-Note 265, Stanford Linear Accelerator Center, 1999.

[37] T. Junk. The 17 hz problem in 1994 data. SLD-Note 245, Stanford Linear Accelerator Center, 1995.

[38] M. Fero et al. Compton polarization measurement: 1995. SLD-Physics-Note 50, Stanford Linear Accelerator Center, 1996.

[39] R. Frey. PGC polarization results for the 1998 run. SLD-Note 266, Stanford Linear Accelerator Center, 2000.

[40] P. Raimondi. Private communications.

[41] P. Emma. Depolarization in the SLC final transformer. Unpublished.

[42] J. P. Fernandez. The chromaticity effect for the 1996-1998 SLD runs. SLD-Note 258, Stanford Linear Accelerator Center, 1999.

[43] Yu. Kamyshkov W. Bugg, Yu. Efremenko. Private communications.

[44] Polymicro Technologies, Inc., 3035 N. 33-d Drive, Phoenix, AZ 85017. *USA Product Catalog.* Product # 300330360.

[45] W. Bugg et al. The QFC polarimeter: Background problem. SLD-Note 255, Stanford Linear Accelerator Center, 1997.

[46] D. Onoprienko. Effect of scattering material in the neutral beam line on the asymmetry measured by the čerenkov Compton polarimeter. SLD-Note 254, Stanford Linear Accelerator Center, 1997.

[47] C. Bula. Test of QED at critical field strength. Presented at 23rd Annual SLAC Summer Institute on Particle Physics: The Top Quark and the Electroweak Interaction (SSI 95), Stanford, CA, 10-21 Jul 1995.

[48] J. Yamartino. A measurement of the e^+e^- decay width of the z^0. SLAC-Report 426, Stanford Linear Accelerator Center, 1994.

[49] P. Rowson P. L. Reinertsen, R. Frey. Event selection for the 1996-98 A_{LR} analysis. SLD-physics-note, Stanford Linear Accelerator Center, In preparation.

[50] P. Rowson. The use of the SLD 120 Hz data to monitor left-right asymmetries in the SLC beam parameters. SLD-Note 244, Stanford Linear Accelerator Center, 1995.

[51] P. Rowson. Update for the 1994/95 SLC run: SLD 120 Hz data analysis. SLD-Note 251, Stanford Linear Accelerator Center, 1996.

[52] I. Ternov A. Sokolov. *Dokl. Akad. Nauk.*, SSSR 153:1052, 1963.

[53] T. Wright H. Band, P. Rowson. Positron polarization measurement. SLD-Note 268, Stanford Linear Accelerator Center, 2000.

[54] K. Abe et al. An improved direct measurement of leptonic coupling asymmetries with polarized Z bosons. Submitted to Physical Review Letters.

[55] T. Takeuchi M. Peskin. *Phys. Rev*, D46:381, 1992.

[56] D. Edwards et al. TESLA test facility linac design report. TTF Report 95-01, DESY, 1995.

[57] The NLC Design Group. Zeroth-order design report for the Next Linear Collider. SLAC Report 474, Stanford Linear Accelerator Center, 1996.

[58] A. Savin et al. Light transport code LTRANS. Unpublished.

Appendices

Appendix A

Quartz Fiber Calorimeter beam test.

After finishing taking data at the SLC Final Focus, the QFC detector was moved to the SLAC Final Focus Test Beam (FFTB) facility for a beam test.

The FFTB was built in 1993 in order to investigate the factors that limit the size and stability of the electron beam at the collision point for a linear collider. It is a straight-ahead extension of the SLAC Linear Accelerator (LINAC). In its primary mode of operation, the FFTB uses a series of magnetic elements and collimators to reduce the size of the beam produced by the LINAC. For the purpose of our beam test, the FFTB was operated in the "parasitic" mode, using a secondary beam produced in the collimators at the end of the LINAC. This way the beam test could be carried out in parallel to other experiments using the LINAC (SLD, PEP-II commissioning).

However, the "parasitic" mode implied serious limitations on our ability to tune the beam and control its parameters. The energy of the beam could be adjusted in the 5 to 25 GeV range. We attempted to take data with the 2 GeV beam but could only collect very limited statistics at that point. The intensity of the beam could be changed from zero to several hundred electrons per pulse. After extensive amount of tuning we were able to focus the beam so that its core had a transverse size between 0.6 and 2.0 mm, depending on the beam energy and intensity, with long tails whose shape and intensity depended on the LINAC running conditions and was very unstable - the fact that significantly complicated the analysis.

The major goals of the QFC beam test were :

- measure the energy response function of the calorimeter. Its linearity is critical for correctly measuring the polarization;
- study the linearity of the detector readout;
- study the effects of the calorimeter misalignment;
- check and tune the Monte Carlo code used for simulating the detector. The simulation is described in the Appendix B.

The rest of this chapter describes the experimental setup, data taking and analysis procedures used for achieving each of these goals. The results are presented in chapter 4 when we discuss the systematic errors of the polarization measurement by the QFC.

A.1 Experimental setup

The scheme of the experimental setup is shown in figure A.1. A system of scintillating counters was used for tuning the beam, rejecting bad machine pulses, and counting the number of particles in a low intensity beam. The "finger" scintillator had a transverse size of 5 by 5 mm, with a thickness of 10 mm. The "paddle" counter had a thickness of 5 mm and a transverse size large enough to cover the whole QFC detector. When the beam intensity was higher than a few particles per machine pulse, it was measured by the Čerenkov counter that had been precisely calibrated by the E144 experiment [47].

The QFC was mounted on a remotely operated micrometer stage that allowed for movement in both vertical and horizontal directions. The calorimeter could also be rotated around a vertical axis. The LED calibration system was used to monitor the phototube gains throughout the run.

A.2 Energy response function

In order to measure the energy response function we took data with a low intensity (about 1 electron per pulse) beam at 6 energy points : 2, 5, 10, 15, 20, and 25 GeV. Requiring that both "finger" and "paddle" counters detect the same number of particles (zero or one) allowed to select high purity samples of "zero incident particles" and "one incident particle" events, with a small size of the "finger" and a large size of the "paddle" providing a guarantee that the particle hit the central region of the QFC, and no particles from the tails of the beam hit other parts of the detector. Consistency

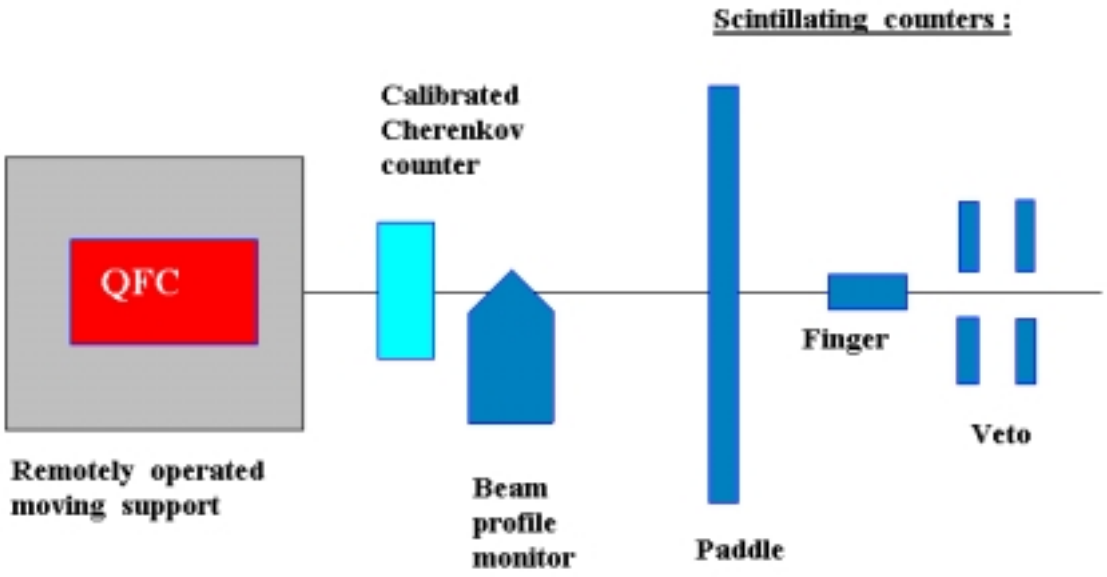

Figure A.1: QFC beam test setup. The "Paddle" and the "Finger" scintillating counters are used to measure the number of electrons in a low intensity beam. At higher beam currents, the beam intensity is monitored by the calibrated Čerenkov lucite counter. The "Beam profile monitor" is a scintillating counter that can be moved diagonally across the beam. This monitor, as well as the "Veto" system, was only used at the first stage of the test to roughly tune the beam. The QFC calorimeter itself was later used for fine tuning.

of the measured response function with linear behavior is illustrated in figure 4.11. In order to calculate the effect on the asymmetry detected by the polarimeter, the response function is convoluted with the dependence of the polarized Compton cross section on the energy of the scattered photon.

A.3 Readout linearity

In order to test the linearity of the detector readout system, we studied the dependence of the detector response on the beam intensity at a fixed energy (15 GeV). The high voltage settings of the QFC readout phototubes during the test were identical to the nominal settings used during the polarization measurement.

The results are presented in figure 4.14 for the X-amplitude channel. It should be noted that the measured dependence is a convolution of the response functions of the QFC and the Čerenkov counter used to monitor the beam intensity. To verify that the observed linear behavior did not result from accidental cancellation of any non-linearities in these two detectors, the study was repeated with different high voltage setting on the Čerenkov counter, and produced essentially identical results.

In order to calculate the effect on the asymmetry detected by the polarimeter, the curve shown in figure 4.14 should be convoluted with the QFC signal distributions observed during the polarization measurement.

A.4 Effects of the detector misalignment

We used the micrometer stage to move the detector across the beam and measure the position dependence of the QFC response, in order to study the uniformity of the calorimeter and the effects of the shower leakages. The data was also taken with the detector rotated by 2.5 degree around a vertical axis. The observed behavior was consistent with the Monte Carlo predictions, but the accuracy of this study was adversively affected by the wide unstable halo around the beam.

Appendix B

QFC polarimeter Monte Carlo simulation.

This appendix owes its existence not only to the role played by the simulation in the eventual success of the QFC project, but also to the number of questions we received about it. I will not describe any particulars of the code, mainly for the reason that I hope not many people will be using GEANT 3 for such relatively large scale and long life simulation projects in the future. If GEANT 4 existed when the project was started, I would happily avoid a laborious and often frustrating job of writing, maintaining, and frequently modifying (to adopt for new tasks) large amount of FORTRAN code. In this appendix, I will describe the goals of the simulation, general approach, and the problems that had to be solved along the way.

The simulation was aimed to:

- Study background situation in the polarimeter area, particularly the background produced by the synchrotron radiation generated by the electron beam in the two dipole magnets located between the Compton IP and the detector. Optimize the detector and shielding geometry to reduce the background.

- Calculate the analyzing powers of the detector channels, taking into account realistic beam shape and the detector geometry.

- Estimate the systematic uncertainties resulting from the effects like angular acceptance, beam size, energy response function nonlinearity, calorimeter misalignment, and local non-uniformities.

- Study potential problems with asymmetry cross-contamination between various detectors located in the polarimeter area.

- Generate fitting functions for the transverse polarization measurement.

While describing the experimental setup geometry accurately and efficiently was relatively straightforward, the following circumstances complicated the simulation:

- Due to the nature of the detector (Čerenkov calorimeter), very large number of events had to be generated to achieve the desired accuracy. For the study of systematic errors, where many modifications of the detector geometry and/or beam parameters had to be tried, computing power limitations presented a serious problem.

- Large region had to be simulated (more than 30 m from the SLD IP to the detector) while accurately representing the tiny details inside the calorimeter (300 μm fiber core diameter).
- Both synchrotron and Čerenkov photons generation and transport routines built into GEANT were highly inaccurate in the versions that existed when the project was started.

To resolve these issues, the simulation was broken into three stages:

1. Initial kinematics generation. Depending on the flags set by the user, the program could invoke either a Compton spectrum generator (with either longitudinal or transverse polarization of the electron beam), or a synchrotron radiation generator (with arbitrary subset of the beam optics magnets turned on). Monochromatic incident beam could also be generated. Beam shape and other parameters could be controlled by the user. The particles were created and transported through empty space (or air) to the detector, then inputed into GEANT. All done by hand, without using any built-in GEANT features. Whenever necessary, pre-generated event databases or parameterizations could be used in this step.
2. Čerenkov light generation and transport in quartz fibers were simulated using the LTRANS package [58], and the results were used to parameterize the light output (more precisely, the average number of photoelectrons created in the phototube) as a function of the incident particle energy, impact parameter, and angle with respect to the fiber axis.

3. Shower simulation in the detector and the surrounding hardware was performed by GEANT. Fiber layers were described as quartz ribbons (no individual fibers). Whenever a charged particle hit such ribbon, readout simulation routine was invoked to determine the readout channel, crossed fibers, and calculate the angle and impact parameters for each fiber. The parametric function created using LTRANS simulation (stage 2) was then used to calculate contribution the detector output signal.

Varying the parameters of the readout simulation routine used in stage 3 described above provided a convenient way to study the effects of local non-uniformities and misalignments in the calorimeter. Late in the experiment, availability of cheap high capacity data storage made it possible to save raw hits generated at stage 3. Created database was used for systematic errors studies, and to generate fitting functions for the transverse polarization analysis. Comparing the ratios of signals in different kinds of the QFC channels (coordinate, amplitude, background) between data and Monte Carlo proved to be very useful for verifying the accuracy of the simulation.

Vita

Dmitry Onoprienko was born in Moscow, Russia on January 16, 1968. He entered the Moscow Institute of Physics and Technology in September, 1985, and graduated with the Master's degree in Physics in June, 1991. After working for a year at the Institute of Theoretical and Experimental Physics in Moscow, he moved to the University of Tennessee, Knoxville, USA, where he participated in the research program leading to the design of the GEM detector for the Super-conducting Super Collider. He returned to the Institute of Theoretical and Experimental Physics in Moscow, Russia, in 1993, and continued work on the High Energy Physics calorimetry related research program. He entered the doctoral program in Physics at the University of Tennessee, Knoxville, in 1995. The Ph.D. degree was received in August 2000.